Conformational changes of the ABC Transporter BmrA Depend on Membrane Curvature

Alicia Damm[1‡], Su-Jin Paik[1§], Raj Kumar Sadhu[1§], Aurélie Di-Cicco[1], John Manzi[1], Michele Castellana[1], Emmanuel Margeat[2], Maxime Dahan[1†], Pierre Sens[1], Daniel Lévy[1]*, Patricia Bassereau[1]*

[1] Institut Curie, Université PSL, Sorbonne Université, CNRS UMR168, Physique des Cellules et Cancer, 75005 Paris, France

[2] Centre de Biologie Structurale (CBS), Université Montpellier, CNRS, INSERM, Montpellier, France

‡ Present address: Laboratoire de Physique de l'Ecole Normale Supérieure, ENS, Université PSL, CNRS UMR 8023, Sorbonne Université, Université de Paris, F-75005 Paris, France

[§] Equally contributed

*Correspondence to: Daniel Lévy (daniel.levy@curie.fr) and Patricia Bassereau (patricia.bassereau@curie.fr)

Abstract

While mechanosensitive ion channels' gating has been well documented, the effect of membrane mechanics, in particular membrane curvature, on the function of transporters remains elusive. Since conical shape transmembrane proteins locally deform membranes, conversely membrane bending could impact their conformations and their function. We tested this hypothesis using BmrA, a bacterial ABC exporter that exhibits large conformational changes upon ATP hydrolysis, switching between open and closed states with opposite V-shapes. After reconstitution in liposomes of different curvatures, we showed that BmrA ATPase activity decreases by 2.9-fold when their diameter decreases from 125 to 29 nm. Moreover, using single-molecule FRET, we observed that the fraction of closed conformations is significantly reduced in highly curved vesicles when adding ATP or non-hydrolysable AMP-PNP. Our results are well explained by a theoretical 2-states model including the effect of membrane mechanics on protein shape transition. Our work reveals that the functional cycle of conical transporters is curvature sensitive, to an extent depending on protein geometry.

Teaser

High membrane curvature strongly impacts the functional cycle of transporters.

MAIN TEXT

Introduction

Transmembrane proteins, being embedded in cell membranes, are prone to react to continuous mechanical deformations due to remodeling and stresses applied to the lipid bilayers. Cells use a large family of proteins, the mechanosensitive channels, to control the permeability of their membrane in response to mechanical stresses. This is the case with the eukaryotic ion channels Piezo[1,2], TRAAK/TREK1[3], and with the prokaryotic Msc family[4], that open at high membrane stretching and allow ions to flow through. It has also been proposed on theoretical basis that these channels could also be sensitive to local high membrane curvature (higher than about 1/50 nm)[5,6], which was confirmed with the Piezo channel[1,7]. The effect of membrane curvature is expected to be enhanced for proteins with an asymmetrical (conical) shape[5], that locally deform membranes[8,9]. Interestingly, some studies have revealed mechanosensitivity upon stretching of proteins with other identified functions, such as the voltage-gated channel KvAP[10]. In fact KvAP has a conical shape[11,12] and locally bends the bilayer[9,13], but only the effect of membrane tension on its function has been explored. We expect that other conical transmembrane proteins are potentially mechanosensitive to membrane curvature. Among them, a sub-group of ABC transporters (ATP-Binding Cassette), known as type IV exporters. These transporters have a domain-swapped arrangement with a V-shape, and are known to be flexible trans-membrane proteins that undergo large conformational changes within the bilayer[14–17]. Moreover, they could locally deform membranes, according to numerical simulations on the human ABC Pgp[9]. These transporters are thus good candidates to test their sensitivity to membrane mechanical properties.

ABC transporters are ubiquitous proteins present in organisms from bacteria to human. They hydrolyze ATP for the transport of a plethora of substrates such as drugs, lipids, ions, peptides (reviewed in [15,18]). They share a commune topology with two transmembrane domains (TMD), two nucleotide-binding sites (NBD) and two intracytoplasmic domains that join TMDs and NBDs. The structure and function of ABCs have been extensively investigated. Type IV ABCs, such as the bacterial lipid exporter MsbA, the Pgp human multidrug resistance protein, or the non-exporter gated chloride channel CFTR, have a "V-shape" apo-conformation and undergo significant conformational changes during their function. A simplified transport mechanism generally involves a two-state mechanism (Fig. 1A): ATP binding to the NBDs induces their dimerisation and switching of the protein from an "open" state - also called "apo"- (referred to as inward facing state in physiological conditions) to a "closed" state (outward facing state respectively) with a tight contact between the NBDs and where the substrate is released. Upon ATP hydrolysis, the protein switches back to its open state and its V-shape. The extent of the conformational change depends on the ABC transporter, but the gap between NBDs can be as large as a few nanometers[16] (Supplementary Fig. S1A and S1B). Importantly, two apo-forms with different NBDs separation have been identified on several ABC exporters, such as Pgp[19], MsbA[20] and BmrA[21–23]. These states are referred to as "wide-open" and "open" (Fig. 1A) and demonstrate a certain flexibility of these proteins, that may depend on the transporter, its substrate and its lipidic environment. Similarly, different sub-states of the two NBDs have been identified, revealing a sequential ATP hydrolysis[21,24].

In this study, based on its large conformational changes, we have selected BmrA, a homodimeric multi-drug resistance exporter from *B. subtillis*, to study the effect of membrane curvature on its function and conformational dynamics. The structures of BmrA in micelle of detergent are known in the closed form[25], highly similar to the closed conformation of other bacterial exporters, with NBDs in close contact and in the wide-open and narrow-open apo conformations[22]. We had previously reconstituted BmrA in lipid membrane at high density and determined a low resolution EM structure, showing an apo conformation with NBDs separated by a few nanometers and a post-hydrolytic state with NBDs in

contact [23,26]. This experiment also revealed a major morphological remodeling of the membrane, from curved to planar, between BmrA reconstituted in apo and closed form in high protein density, respectively[26]. This demonstrates BmrA's ability to bend a membrane depending on its state. The apo- and closed-conformations correspond to two different conical shapes of the transporter with a conicity of 15° to 28° ($\pi/12$-$\pi/7$) in the apo conformation depending on the separation of the NBDs, and an opposite value of -17° (- $\pi/10$) in the closed one (Supplementary Fig. S1C). Altogether, we expect that substantial conformational changes of individual BmrA within the membrane will lead to local membrane deformations, dependent on its conicity during its ATP cycle. Conversely, the conformational changes and function of BmrA should be modulated by membrane curvature.

Practically, snapshots of ABCs' conformations have been derived with structural techniques (X-Ray, NMR and more recently cryo-EM)[16,27]. Moreover, dynamical conformational changes have been detected on different ABCs, such as the bacterial BmrCD[28], MsbA[19,29] and McjD[30] or the human Pgp[31–33], CFTR[34] and MRP1[35] with DEER, LRET or smFRET. Most of these studies were performed on proteins solubilized in detergent micelles or embedded in ~ 10 nm lipid nanodiscs, where the effect of membrane curvature cannot be addressed. Only four have reported ABC exporters in liposomes, but have not considered the effect of vesicle size[29,30,33,34]. Here, we have reconstituted BmrA in Small Unilamellar Vesicles (SUVs) in two populations with small and large diameters. First, we have measured a reduction of ATPase activity for the smallest liposomes. Next, after fluorescent labeling of BmrA on specific NBD residues where the distance is the largest in the apo form, we used TIRF microscopy on immobilized liposomes to detect conformational changes with smFRET. We observed an open (apo) conformation, and a closed one in the presence of ATP or of a non-hydrolysable ATP (AMP-PNP). Interestingly, the fraction of proteins in closed conformation decreases in both cases with increasing membrane curvature, consistent with the observed decrease in activity. Moreover, we propose a theoretical model based on membrane mechanics to quantitatively predict the role of membrane shape and elasticity in the control of the ATPase activity of ABC transporters.

Results

BmrA ATPase activity decreases with increasing membrane curvature

We first purified BmrA in detergent (N-dodecyl-β-D-maltoside (DDM)) and reconstituted it in small unilamellar vesicles (SUVs) made of 90% (w/w) Egg Phosphatidyl Choline (EPC) doped with 10% of brain Phosphatidyl Serine (bPS), a negatively charged lipid known to stimulate the ATPase activity of some ABC transporters[36]. BmrA (with a molecular weight M = 130 kDa for the homodimer) was incorporated at 1:13000 molar (homodimer) Protein Lipid Ratio (PLR) (see Materials & Methods for detailed protocols). We found that by adjusting the SUVs preparation temperature, we could obtain two different size distributions of the proteoliposomes, which we characterized by cryo-EM (Fig. 1B): i) upon preparation at 20°C, a broad distribution of large vesicles "LV", with a diameter ø = 123 ± 41 nm; ii) upon reconstitution at 4°C, a narrow distribution of very small vesicles "SV", with a diameter ø = 29 ± 6 nm. Importantly, the conformation of the reconstituted protein, in apo form or in the presence of ortho-vanadate (Vi) (a commonly used inhibitor that prevents from the NBDs dissociation) had no impact on the size of the small liposomes (ø = 29 ± 6 nm with apo BmrA and ø = 30 ± 6 nm for ATP-Vi BmrA). Moreover, these cryo-electron microscopy images showed that liposomes were unilamellar without multilamellar vesicles (Fig. 1B). Finally, we showed that vesicles' size and unilamellarity remained unchanged after being exposed for a long time to different temperatures in the course of our

experiments (37°C for the ATPase activity measurements and 20°C for smFRET experiments described further) (Supplementary Fig. S2).

With floatation in sucrose gradient, we measured 90-95 % protein incorporation in both samples (middle and top fractions) without aggregated proteins in the bottom fraction (Fig. 1C). Finally, by cleaving the NBD with trypsin, we showed that for LV and SV respectively, 85% and 75 % of the proteins had their NBDs facing outside the liposomes, respectively, thus accessible upon addition of ATP in the external medium (detailed protocol in Materials & Methods, Fig. 1D). Thus, proteoliposomes were similar in lamellarity, amount and orientation of incorporated proteins and differed only by their size.

Using a standard enzymatic assay (see Materials & Methods), we measured the ATPase activity *A* of BmrA in detergent micelles and after reconstitution in proteoliposomes in the presence of 5 mM ATP. Note, we performed our experiments without a substrate since BmrA activity is weakly dependent on its presence[18,37]. The activity was 0.17 µmol ATP/min/mg of protein in DDM and significantly increased after reconstitution in vesicles, as reported for BmrA and several ABC transporters[26,38,39]. However, after reconstitution (PLR=1:13000 molar), the ATPase activity strongly decreased when reducing the liposome size. Indeed, at 37°C, we measured a 2.9-fold lower activity in the highly curved liposomes SV (*A*=1.7 µmol ATP/min/mg of protein), as compared to the larger vesicles LV (*A* = 5 µmol ATP/min/mg of protein) (Fig. 1E); this corresponds to a turnover τ = 543 ms in SV and τ = 185 ms in LV for the hydrolysis of one ATP molecule per BmrA molecule, respectively ($\tau = 60.10^3/A \times M$, in seconds, with *M* the protein molecular weight). The activity is comparable to previously published data on liposomes containing BmrA (~6 µmol of ATP/min/mg)[37] or the closely-related ABC transporter MsbA (~5 µmol of ATP/min/mg)[38]. By measuring the activity for ATP concentrations ranging between 0.1 mM to 5 mM, we have confirmed that for both vesicle populations SV and LV, 5mM ATP corresponds to saturating conditions (Supplementary Fig. S3). Our data show that membrane curvature strongly impacts BmrA activity; however, the protein is able to maintain its cycle in spite of the mechanical stress experienced in the context of the small liposomes. To further decipher the consequences of this strain on the protein conformational changes, we have next investigated the effect of membrane curvature on BmrA structure using single molecule FRET.

Single-molecule FRET assay to monitor the conformational dynamics of BmrA in LV and SV liposomes

In order to fluorescently label the homodimeric BmrA for smFRET experiments (Fig. 1A), we used the two native cysteines C436 located at the basis of the NBDs, close to the TMDs, for which the distance change during the protein cycle, thus the FRET change, are expected to be the largest (Supplementary Fig. S1A and S1B). Among other FRET pairs that we have tested, sulfo-Cy3/sulfo-Cy5 happened to be the most suitable in terms of photochemistry, labelling ratio, and protein activity preservation (Materials & Methods; Supplementary Fig. S4). The activity of the labelled proteins was conserved at 80% as compared to the non-labelled protein. Moreover, due to the homodimeric nature of BmrA, 25% of the proteins carry both fluorophores (see details in Materials & Methods).

Our FRET experiments were performed using TIRF microscopy with alternating laser excitation (ALEX) at 532 nm (Donor = sCy3) and 638 nm (Acceptor = sCy5)[40]. We measured the intensities I_D, I_F and I_A of single molecules versus time in the Donor, FRET and Acceptor channels, respectively, with an acquisition rate of 1/200 ms^{-1}. Upon following selection criteria (described in Materials & Methods), we retained data points corresponding to molecules labelled with both a donor and an acceptor, for which we measured over time the apparent uncorrected FRET efficiency $E_{app} = \frac{I_F}{(I_F+I_D)}$ until either the

donor or the acceptor bleaches (an oxygen scavenger solution was used to limit bleaching). We then plotted the distribution of instantaneous E_{app} values from multiple traces (total number of proteins N_{prot} > 100), and performed a single or double Gaussian fit, extracting a peak mean position $<E_{app}>$ and a width parameter *w* (equation and parameters are defined in Material & Methods). The sensitivity of our system was checked with a well-established assay[41,42] (Supplementary Information; Supplementary Fig. S5; Supplementary Table S1), using three 40 base-pair double-stranded (ds) DNAs, carrying the same donor/acceptor pair, at distances ranging between 3 and 7 nm, similar to interdye distances on BmrA and its homologs (Supplementary Fig. S1A and S1B).

We have next implemented a parallelized FRET assay where the conformation of single proteins embedded in multiple liposomes immobilized on a glass substrate can be followed over time (protocol adapted from [43]). The liposomes, containing 0.5% of biotin-PEG-DSPE, were immobilized onto custom-made flow cells, extensively cleaned to get rid of fluorescent contamination (Supplementary Fig. S6A) and pre-treated with silane-PEG-biotin and neutravidin (Supplementary Fig. S6B). The specificity of this tethering strategy was confirmed since very few liposomes are bound to the surface in the absence of neutravidin (Supplementary Fig. S6C). Typical microscopy images of Donor and FRET channels are depicted on Supplementary Fig. S6D. Single molecule experiments require to have maximum one protein (homodimer) per liposomes. In practice, we aim for having about one tenth of liposomes containing a protein, reducing the probability to have two proteins per liposome to 1%. To determine the concentration of protein required to be in this regime, we have incorporated sCy5-labelled BmrA in fluorescently labelled SV liposomes with 0.01% of BODIPY®-FL-C5-HPC lipid, which allowed detecting simultaneously the liposomes and the proteins (Fig. 2A). For PLR= 1:81200, we found that 40% of vesicles co-localized with sCy5-BmrA while 60% did not contain any protein. For PLR= 1:406000, only 5% of the liposomes contained a protein. We have thus reconstituted the transporter at PLR= 1:326000 in the SV, and PLR= 1:650000 in the LV. Finally, we established that the bound vesicles remained sealed and non-permeable to small molecules by encapsulating the soluble dye pyranine in the liposomes labelled with 0.5% of Texas Red® DHPE (Fig. 2B). Co-localization of both fluorescent signals indicated that up to 80% of liposomes were intact after tethering to the surface. We found that the percentage of intact liposomes decreased when increasing the PEG-Biotin density on the surface, due to membrane ripping open. We selected a PEG-Biotin density of 1% for our experiments. Finally, we noted that the average fluorescence lifetime of the dyes was much shorter when linked to BmrA than to the DNA molecules (Supplementary Informations; Supplementary Fig. S5D and S5E), on average 7 seconds for labelled-BmrA while DNA could be observed up to several tens of seconds, even in the presence of the same oxygen scavenger system (Materials and Methods). This effect could be due to an enhanced photostabilization of the cyanines dyes upon interaction with the DNA bases[44].

BmrA exhibits two conformations upon addition of ATP analogs

It is largely reported that type IV ABC exporters switch between two extreme states during the transport cycle: i) a nucleotide-free apo-form where the NBDs are separated by a distance that depends on the ABC and ii) a closed form with dimerized NBDs upon nucleotide binding (e.g. ATP)[14]. The lifetime of the closed conformation can be significantly increased by using ATP analogs in the presence of Mg^{2+}. Two commonly used ones are AMP-PNP and ortho-vanadate (Vi)[45] (described on Fig. 1A). AMP-PNP is a non-hydrolysable form of ATP, which binds to the NBDs and leads to their dimerization with the protein in a pre-hydrolytic conformation. This binding is reversible, but since it does not involve ATP hydrolysis, the NBDs remain dimerized for a longer time than with ATP. In contrast, in the presence of ATP, ortho-vanadate is expected to form covalent bonds with the ADP phosphate group bound to the NBD, preventing it from being released and therefore maintaining the protein in a closed post-

hydrolytic form and inhibiting its ATPase activity. We first confirmed the effect of both compounds on BmrA in vesicles: BmrA activity in the presence of 5mM ATP is strongly reduced by 80 % upon addition of 2 mM vanadate (ATP-Vi) (well above K_m=0.05 mM[37]), and by only 25% while adding 5 mM AMP-PNP (Supplementary Fig. S7).

We have then used our single-molecule assay to measure the FRET efficiency and thus the conformations of single BmrA molecules in the presence of ATP-Vi or AMP-PNP in the SV and LV liposomes. In both cases, the analogs were added *prior to reconstitution* at a concentration of 5 mM to the mix of protein/lipid in detergent. In order to work at constant nucleotide concentration and reduce dissociation due to nucleotide depletion, the analogs were kept at 5mM in the observation buffer during the smFRET experiments.

In the presence of Vi that inhibits BmrA activity by 80%, we expected to observe mainly a high FRET conformation, corresponding to the closed state of the dimer. Surprisingly, the FRET efficiency histograms exhibited a two-peak distribution in both LV and SV populations (Fig. 3A; 2D histograms with apparent efficiency E_{app} and stoichiometry S_{app} are available on Supplementary Fig. S8; Table 1). This demonstrates the co-existence of two states: i) a high FRET peak at $<E_{app}>$ = 0.45, corresponding to the closed state with an interdye distance of about 4 nm from known structures[25] (Supplementary Fig. S1); ii) a low FRET $<E_{app}>$ = 0.10, corresponding to an open conformation where the NBDs are separated about 7 nm according to the recent structure[22]. Note that, as we suspected, we cannot distinguish between a wide- and a narrow-open conformation, due to the smFRET resolution in this distance range. We thus call this low FRET population "open" (Fig. 1A). From the two-Gaussian fit, we extracted the respective weight of the low and high-FRET populations; we found that they have the same weight for both LV and SV, around 50% (Table 2). Importantly, no transition was detected between the open and closed state on individual time traces (Fig. 3C-D). This result is also enforced by measuring the time average FRET efficiency per protein (Supplementary Fig. S9): the histograms present the same low and high-FRET populations. Altogether, this shows that half of the proteins are open, and half are closed during the time of our experiments, independent of the size of the liposomes. Considering the high activity of our BmrA preparation (about 3 times higher than in [46]), this is probably not due to a dead fraction. Moreover, since the open fraction is the same for LV and SV, the effect of membrane mechanics can also be discarded. Note that, although surprising, such a co-existence of open and closed conformation in ATP-Vi has previously been reported, in nanodiscs and detergent, for BmrA in ensemble experiments[47], for its bacterial homolog MsbA[19], human homolog Pgp[32], and for the heterodimer BmrCD[28].

For proteins reconstituted in the presence of 5 mM AMP-PNP, we also observed a bimodal distribution with peaks at similar positions as in the presence of ATP-Vi, showing the co-existence of the same open and closed states: one at low FRET ($<E_{app}>$ = 0.15 for the LV and $<E_{app}>$ = 0.16 for the SV) and one at high FRET ($<E_{app}>$ = 0.47 for the LV and $<E_{app}>$ = 0.43 for the SV) with no switch between these conformations (Fig. 3B; Table 1; Supplementary Fig. S8 and S9). However, the relative fractions of these states are different from the ATP-Vi condition. First, the fraction in the closed state P_{cl} is lower in AMP-PNP (32% in LV and 21% in SV) (Table 2) than in presence of ATP-Vi (50%), in line with our activity measurements in detergent showing a stronger inhibition by ATP-Vi. Similar differences between these analogs were reported on human ABC Pgp[32,48] or ABCB7[49]. Second, in contrast with the ATP-Vi, the fraction in a closed state is reduced by about 30% in the smallest liposomes SV as compared to the population with a larger size. Altogether, this suggests that, in the presence of AMP-PNP where closed and open forms are in equilibrium, the NBDs dimerization rate depends on membrane curvature, which is not the case when NBDs irreversibly dimerize in complex with ADP:Vi.

The fraction of BmrA in closed conformation decreases with membrane curvature

We then investigated the conformational changes of BmrA during its ATPase cycle. We first assessed the apo-BmrA conformation (in the absence of ATP) when reconstituted in LV and SV liposomes (Fig 4A-B top histograms; Supplementary Fig. S8). As expected, we observe a peak at low FRET for both vesicle sizes. Although these distributions would be fitted with a single Gaussian (Supplementary Fig. S10), a better fit was obtained (notably for SV) with a double Gaussian while fixing the position of a second peak at 0.45, as measured above with the ATP analogs. In this case, we found that a large majority of proteins (92 % for the LV and 86% for the SV (Table 2)) are in the open conformation. The low FRET peak is centered at $<E_{app}> = 0.11$ for the LV and $<E_{app}> = 0.14$ for the SV (Table 1), similar to the low-FRET state observed under addition of ATP analogs. This demonstrates that apo-BmrA exhibits an open conformation in vesicles, independent of membrane curvature.

We finally studied the effect of ATP on the conformational distribution. Interestingly, upon addition of 5mM Mg-ATP, we observed differences between the two vesicle populations (Fig. 4A-B bottom histograms; Supplementary Fig. S8). As above, we analyzed the FRET distributions with a double Gaussian and by setting the high-FRET peak at 0.45 (parameters in Table 1). We found that the position of the peak corresponding to the open form remains essentially unchanged, 0.13 for the LV and 0.12 for the SV. However, as compared to the apo condition, we detected a second high-FRET population corresponding to the closed form, with a fraction P_{cl} that depends on the SUV size. Addition of ATP resulted in an increase of 13.1% of closed protein population compared to the apo form for the LV, but only in 4.1% for the SV (Fig. 4C; Table 2), significantly lower than for the LV. Though a rare observation, we detected a switch between both conformations on some traces (examples are in given in Supplementary Fig. S11A and S11B, where ATP-induced conformational dynamics is visible, as compared to traces where the proteins was stably found in closed conformation, displayed on Supplementary Fig. S11C and S11D): 2 times over 226 proteins for the LV and 3 times over 130 proteins for the SV. Despite the oxygen scavenger present in our buffer, the traces recording lasted 7 seconds on average before bleaching. To summarize, the analysis of the traces shows that BmrA proteins are either open or closed for a few seconds in the presence of ATP (Supplementary Fig. S11C and S11D). In conclusion, we show here that high curvature reduces the probability of the protein to be in a closed state, in agreement with a reduced ATPase activity measured at the ensemble level.

Modeling the effect of membrane curvature on the open to close transition probability

We then have developed a model to quantify the influence of membrane mechanics on the cycle of conformational change of BmrA. In order to simplify the theoretical description, we assume that the change of protein conformation can be described by a single reaction coordinate, the V shape angle θ (Fig. 4D). In the absence of nucleotide, the protein energy landscape $E_p(\theta)$ is assumed to have a minimum in the open (apo) conformation θ_{op}, which we model for simplicity as a quadratic energy with a stiffness A: $E_p(\theta) = A\left(\theta - \theta_{op}\right)^2$ (Fig. 4E). Thermal fluctuations can bring the protein to its closed conformation θ_{cl}, and if nucleotides are bound to the two NBDs, the landscape gains a deep minimum at θ_{cl} characterized by a binding energy ε when the NBDs bind to one another. We may consider two types of nucleotides, ATP or the non-hydrolysable AMP-PNP. With ATP, the binding energy is assumed to be so large that the protein remains in the closed conformation until ATP hydrolyses, which occurs at a prescribed rate k_{ATP}. With AMP-PNP, the system is considered to be at thermodynamic equilibrium and the closed-open transition occurs when thermal fluctuations bring the protein over the energy barrier ε. Membrane mechanics modify the transition rates through the energy of membrane deformation associated to the protein shape changes. This term depends on the membrane's bending rigidity and on the geometry of the liposome in which the protein is embedded

(Supplementary Fig. S12). Membrane shape optimization can be performed analytically under the assumption of small deviations from a spherical shape (all details of the model are provided in Supplementary Information). Under this condition, we find that the membrane energy scales as $E_m(\theta) = 2\pi\kappa\left(\frac{a}{R}\right)^2(\theta-\theta_R)^2$, where κ is the membrane's bending rigidity, a and R are the protein and SUV radii, and the optimal opening angle is $\theta_R = sin^{-1}(a/R) \approx a/R$ if the SUV is in the optimal state and have a spontaneous curvature $2/R$.

In the thermal equilibrium case, the probability ratio of open P_{op} and closed conformation P_{cl} follows a Boltzmann statistic. In the non-equilibrium case (when ATP is hydrolyzed), this ratio has a steady-state value given by the balance between the thermal flux (from the open to the closed conformation) and the active reversed flux. Writing $\Delta E_i = E_i(\theta_{cl}) - E_i(\theta_{op})$, we find:

$$\textit{Equilibrium: } \frac{P_{op}}{P_{cl}} = e^{\left(\Delta E_p+\Delta E_m(R)-\varepsilon\right)/kT} \;\mid\; \textit{Non-equilibrium: } \frac{P_{op}}{P_{cl}} = \frac{k_{ATP}}{k_0}e^{\left(\Delta E_p+\Delta E_m(R)\right)/kT} \qquad (1)$$

where kT is the thermal energy and k_0 is a typical rate of thermal fluctuation of the protein conformation. In the non-equilibrium case, one can also derive the rate of ATP hydrolysis per protein $1/\tau$ as:

$$\frac{1}{k_0\tau} = \frac{k_{ATP}/k_0}{1+(k_{ATP}/k_0)e^{\left(\Delta E_p+\Delta E_m(R)\right)/kT}} \qquad (2)$$

Through the energy difference $\Delta E_m(R) = 2\pi\kappa\left(\frac{a}{R}\right)^2(\theta_{op}-\theta_{cl})\left(2\frac{a}{R}-\theta_{cl}-\theta_{op}\right)$, Eqs.(1,2) provide the size-dependence of the open and closed populations, as well as the rate of ATP hydrolysis. As the open conformation is facing outward, we expect $\theta_{op} > 0$ and $\theta_{cl} < 0$ and $\Delta E_m > 0$ for liposomes with large curvature (Supplementary Fig. S1C). Therefore, we expect the closed conformation to be disfavored, and the rate of ATP hydrolysis to be lower for the smaller SUVs (SV) compared to the larger ones (LV). Note that a proper description of the experimental observation must account for the fact that each sample contains a distribution of vesicle size, as well as a fraction of proteins with inward-facing NBDs (Theoretical section of the Supplementary Information) (Supplementary Fig. S13), which we found not to affect significantly our conclusions.

One important prediction of the model is that the open-to-close probability ratio for the two distributions of vesicle size are related by a Boltzmann factor that only involves the membrane deformation energy ($e^{\left(\Delta E_m(V20)-\Delta E_m(V125)\right)/kT}$) both in the equilibrium (AMP-PNP) and non-equilibrium (ATP) case. This prediction agrees with our observations (Fig. 4F, top; Supplementary Fig. S13A), with $\Delta E_m(SV) - \Delta E_m(LV) \simeq (0.7 \pm 0.2)kT$. Based on BmrA and homologs' structures, we used a protein diameter $2a \approx 4nm$ (Supplementary Fig. S1D). Since the conicity of the closed conformation is independent of the protein membrane environment[19,32], θ_{cl} was set to $-\pi/10$ measured from closed BmrA structure in detergent (Supplementary Fig. S1C). Conversely, it was reported that the opening of the apo form of homologs MsbA and Pgp changes between detergent and nanodisc environments[19,32]. Therefore, we used $\theta_{op} \approx +\pi/10$, corresponding to MsbA structure in membrane (nanodisc), in good agreement with the angle measured for BmrA in vesicles at high protein density but low resolution[23] (Supplementary Fig.S1A and S1C). Fitting our data with these parameters leads to a membrane bending rigidity $\kappa \approx (21 \pm 5)kT$, which is in line with expected values[50]. Note that $\Delta E_m/kT$ is very small for large SUVs ($\simeq 6 \cdot 10^{-3}$) so that proteins are not sensitive to membrane elasticity, while the open-to-closed transition should be moderately impaired in the smaller SUVs ($\Delta E_m/kT \simeq 0.7kT$), as observed. Knowing the membrane parameters from the previous fit, we can determine the value of the relevant combination of protein parameters in the active case for the chosen ATP concentration:

$(k_{ATP}/k_0) \cdot e^{\Delta E_p/kT} \simeq 5$. This lets us predict how the protein activity (the rate of ATP hydrolysis) depends on the liposome size (Fig. 4F, bottom; Supplementary Fig. S13B). In the case of our experiments, we predict that it is reduced by about 50% for the small SUVs as compared to the larger ones, a value in very good agreement with the experimental value obtained from ensemble measurements (Fig. 4F, bottom).

Discussion

In general, mechanosensitive membrane proteins have been identified through the cell response after mechanical stresses and then, the corresponding molecular mechanism linked to their function studied at the structural level. Previous studies on MsbA[29] and on ABC importers OpuA[51] and ButCD[52] have highlighted the effect of the local environment for ABC transporters, showing at the single-molecule level different degrees of opening of the apo conformation when incorporated in detergent or in lipid nanodiscs. Our smFRET study reveals for the first time that membrane curvature also impacts the conformation of an ABC transporter, as well as its activity. Our experiments, in which we control the curvature of liposomes, demonstrate that the activity of BmrA decreases when increasing membrane curvature, as well as the fraction of proteins in a closed conformation. These results can be recapitulated with a theoretical model based on the idea that the protein conformation changes are associated to membrane deformation and are therefore sensitive to membrane mechanics. As in our experiments, the curvature of the liposome membrane fits the outward facing open conformation better than the closed conformation, membrane energy favors the open state. In cell, the open conformation is inward facing (toward the cytoplasm), so that the effect of membrane energy should be opposite. It should favor the transition from open to closed conformation and increase the protein's activity. We expect this effect to be relatively small for BmrA owing to the small value of the product of the cell curvature times the protein size.

Regarding the open conformation, a wide range of openings have been reported among ABC exporters, with NBDs in close contact up to NBD separated by about 6-7 nm[14,16,27,53]. Our smFRET data in vesicles are consistent with the recent 3D model of BmrA in detergent[22] with dissociated NBDs in the apo form. However, we have not detected any difference for the low FRET between LV and SV, in contrast with the transition rate between both conformations. Former studies on bacterial MsbA and human PgP stressed that this relative opening is wider in detergent than in lipid nanodisc[19,32], suggesting that the protein environment influences the structure of these transporters. In our model, using the open angle $\theta_{op} \approx +\pi/7$, deduced from the BmrA structure in detergent (Supplementary Fig. S1C), led to a membrane bending rigidity $\kappa \approx (29 \pm 7)kT$, when fitting to the population and activity curves. For the full range of liposome size we explored, θ_{op} is larger than the optimal opening angle fixed by the vesicle size θ_R, so that the energy difference ΔE_m decreases with θ_{op} in this regime (see Eq. 11, SI theory), hence a higher fitted value of κ. For a more detailed comparison with our model, experiments where the single molecule FRET traces would be measured simultaneously with the corresponding liposome diameter deduced from membrane fluorescence[54] would be optimal, though challenging in single molecule experiments due to fluorescence leaking.

Our activity measurements have highlighted that the turn-over of ATP-hydrolysis increases from 0.18 s to 0.54 s between the LV and SV liposomes. In principle, by monitoring smFRET over a few seconds, we anticipated to detect conformational dynamics, which was not the case. Experimentally, activity was measured at 37°C, while smFRET experiments were performed at room temperature in order to limit evaporation in the small observation volumes used. In these conditions, a reduction of activity by only

a factor about 4 was expected, based on previous measurements on Pgp[55]. In fact, for BmrA, with our ATPase assay, we found out that its activity is reduced by a factor 20 over this temperature range (Supplementary Fig. S14). Hence, this explains the slow turn-over in our smFRET experiments and the low probability of detecting conformational transitions. Nevertheless, by measuring the average lifetime of the proteins in the high-FRET state in LV (with $E_{avg} > 0.3$, N = 38 proteins /226), we can conclude that in these conditions and at 20°C, the lifetime of the closed state is longer than 7 seconds. This value is of the same order of magnitude than the average turnover measured in cuvette for the LV and SV (respectively 3.7 and 7 seconds). Similarly, at room temperature, lifetime of a few seconds was found for the closed state of McjD[30] and more recently of the human ABC CFTR[34].

Our model predicts that such an effect of membrane curvature can be expected for all type-IV ABC exporters, provided that the apo form is sufficiently open, since they have similar size and well-conserved closed conformations. From the model, we infer that ABCs with BmrA characteristics are mechanosensitive only at large membrane curvature, higher than 0.08 nm^{-1} (i.e. for liposomes smaller than 40 nm diameter), and that this property is negligible in vesicles with diameter bigger than 70 nm. The human Pgp being a close homolog to BmrA (Supplementary Fig. S1), we expect that membrane bending should not affect its function in usual transport vesicles inside cells, or endosomal compartments. Nevertheless, significant effects should be detected at weaker curvature for proteins with a larger membrane imprint (a) and/or with higher conicity (θ_{op} and θ_{cl}) (Supplementary Fig. S15). Membrane bending rigidity (κ) can also modulate the conformational switch (Eq. (2)). Consequently, changing membrane stiffness by adjusting lipid composition (e.g. via cholesterol or sphingomyelin concentration) is expected to tune the sensitivity of the activity to membrane curvature; however, lipid composition by itself can also affect protein activity[56].

Altogether our results demonstrate that membrane curvature plays a role in the transport cycle kinetics of ABC transporters. This invites us to re-think the definition of *mechanosensitivity* to also include other proteins whose activity involves large shape changes within the membrane. BmrA's sensitivity to membrane bending suggests a potential response to membrane tension. However, curvature and membrane tension could have different consequences. While the effect of membrane tension on mechanosensitive proteins has been largely documented, it would be worth to investigate the effect of tension on the function of this new class of mechanosensors.

Materials and Methods

Reagents

Egg Phosphatidylcholine (EPC), brain Phosphatidylserine (bPS), 1,2-distearoyl-sn-glycero-3-phosphoethanolamine-N-[biotinyl(polyethylene glycol)-2000] (DSPE-PEG(2000)-Biotin) and 1,2-dihexadecanoyl-sn-glycero-3-phosphoethanolamine, triethylammonium salt (Texas Red® DHPE) were from Avanti Polar Lipids (Alabaster, AL, USA). All lipids were purchased in CHCl3 stock solution. BODIPY®-FL-C5-HPC was purchased from Invitrogen. N-dodecyl-β-D-maltoside (DDM) and Anapoe® X-100 (Triton® X-100) were purchased from Anatrace (Maumee, OH, USA). 50 mesh BioBeads® were purchased from Bio-Rad (Hercules, CA, USA) and prepared according to [57]. Lacey carbon electron microscopy grids were purchased from Ted Pella (Reding, CA, USA). Nucleotides, ATP, AMP-PNP, ATPase inhibitor orthovanadate, pyranine and all other chemicals were purchased from Sigma Aldrich (Merck KGaA, Darmstadt, Germany). SulfoCy3 and SulfoCy5 maleimide probes were purchased from Lumiprobe GmbH (Germany). Coverslips for the custom-built chambers were purchased from Menzel-Gläser (Germany) (thickness #1). Silane-PEG2000 and silane-PEG3400-biotin

were purchased in powder from LaysanBio (Alabama, USA) and dissolved in DMSO. Neutravidin and (from bovine milk > 98%) were purchased from Sigma Aldrich (Merck KGaA, Darmstadt, Germany). Double stranded DNA for FRET calibration was purchased from Eurofins Genomics (Ebersberg, Germany). D-glucose, glucose oxidase and Trolox were purchased from Sigma Aldrich. Catalase from bovine liver was purchased from MP Biomedicals (California, USA).

BmrA expression, purification and labelling

His-C-ter-BmrA was expressed in *E. coli* and purified in 0.05 % DDM as previously reported[23]. Elution buffer from Ni-NTA agarose beads was 50 mM Tris, pH 8.0, 100 mM NaCl, 250 mM imidazole, pH 8.0, 10% glycerol, 0.05% DDM. Proteins were eluted at 0.3-1.5 mg/mL and used without further concentration as it caused protein aggregation (observed in EM). Purified proteins were aliquoted in 50 µL volume and kept at -80°C before use. Aliquots were thawed only one time before experiments. Protein concentration was measured by Bradford method.

For smFRET experiments, purified BmrA collected from elution step was fluorescently labelled using maleimide dyes on C436, the sole Cys residue, and thus two C436 were labeled per homodimer of BmrA. Several couples of donor/acceptor dyes were evaluated according to the rate of labelling and the ATPase activity of the labelled proteins including Alexa488/Atto610, Alexa488/sulfoCy5, Cy3B/sulfoCy5 and sulfoCy3/sulfoCy5 selected based on spectrum overlap, dye photostability and published data. Best results have been obtained with sulfoCy3/sulfoCy5. BmrA in detergent was incubated with sulfo-Cy3 and sulfo-Cy5 maleimide dyes, at sCy3/sCy5/protein 10/10/1 mol/mol/mol, overnight at 4°C (Supplementary Fig. S4). Thiol-maleimide reaction was performed at pH 7. Unbound dyes were removed by binding BmrA at pH 8 on Ni-NTA agarose beads in batch followed by washing with 5 volumes of a free dye buffer before elution with 250 mM imidazole. Labeled BmrA was analyzed on SDS-PAGE gel by fluorescence and stained with Coomassie blue. The rate of labelling was calculated from the concentration of fluorescent dyes measured by absorbance of sCy3 (molar extinction coefficient ε_{max} = 162 000 $cm^{-1}.M^{-1}$), sCy5 (ε_{max} = 281 000 $cm^{-1}.M^{-1}$), and from the protein concentration measured by Bradford assay. We found 32% of labelling for sCy3 and 39% for sCy5. BmrA is a homodimer and we have labeled the two C436 residues with maleimide-conjugated dyes. Therefore, we can calculate that statistically, we have the following labeling probabilities: not labelled 8%; single-labelled sCy3 19%; doubly-labelled sCy3/sCy3 10%; single-labelled sCy5 23%; doubly-labelled sCy5/sCy5 15%; doubly-labelled sCy3/sCy5 25%. ATPase activity was measured as described below and sCy3/sCy5 labelled BmrA retained 80% of the unlabeled protein.

Reconstitution of BmrA in proteoliposomes

Proteoliposomes containing BmrA were formed by detergent removal using Bio-Beads® from a fully solubilized mixtures of lipid/protein/detergent, as reported previously[37] and according to the principle reviewed in [58,59]. We first prepared pure lipid liposomes composed of EPC:bPS 90:10 w:w, supplemented with 0.5% of biotin-PEG2000-DSPE to allow liposomes immobilization for the smFRET study. A dried lipid film was obtained by evaporating organic solvents from the lipid mix. Lipids were then resuspended in water at 10 mg/mL, sonicated with a tip sonicator for one minute while keeping the solution on ice. 50 µL aliquots were made and samples were kept frozen at -20°C. For each reconstitution, an aliquot of lipid vesicles was resuspended at 2 mg/mL in 50 mM MOPS, 150 mM NaCl, 1 mM $MgCl_2$, pH 7.5, then lipids were solubilized with Anapoe® X-100 for 15 minutes at detergent/lipid ratio of 2.5 w:w. It is worth noting that BrmA is stable and functionally active both in Anapoe® X-100 and in DDM, allowing the use of different detergents for lipid solubilization and purification of BmrA. After lipid solubilization, BmrA was added at a protein to lipid ratio (PLR) of 1:650000 for LV and 1:325000 for SV. This PLR ensured that less than one BmrA homodimer was

incorporated per proteoliposome. For AMP-PNP and ATP-Vi experiments, inhibition of the protein was performed upon addition of 2 mM orthovanadate (Vi) and 5 mM ATP, or of 5 mM AMP-PNP, in the presence of 5 mM $MgCl_2$ in the buffers. The solution was incubated for 15 minutes, then detergent removed by the addition of BioBeads® under gentle stirring. Detergent removal was performed at 20°C and 4°C respectively to produce the LV and SV populations. The BioBeads® were added in three rounds at the following BioBeads®/ Anapoe® X-100 ratio: i) for the LV population, 10 w:w for 2h, then 10 w:w for 1h and 20 w:w for 1h; ii) for the SV population, 30 w:w for 2h, then 30 w:w for 1h and 60 w:w for 1h. Note that the amount of BioBeads® was increased during the reconstitution at 4°C (SV) to ensure that the rate of detergent removal was similar than at room temperature. These amounts of BioBeads® were sufficient to remove all detergent molecules including the amount of DDM present in the preparation of BmrA[60]. As also shown previously, at this low PLR, negligible amounts of lipid and no protein were adsorbed onto the BioBeads®[61]. After detergent removal, the reconstituted supernatants were removed and stored for no more than 24h at 4°C before analysis. It is worth noting that ATPase activities were stable for at least 24h at 4°C as proteoliposomes remained unchanged as seen by cryo-EM.

Protein incorporation and orientation in proteoliposomes

Protein incorporation in the population of vesicles was measured after separation of proteoliposomes, aggregated proteins and protein-free liposomes by sedimentation in a sucrose gradient according to a protocol modified for proteoliposomes[62]. BmrA was reconstituted at PLR=1:9750 in EPC-PS 9/1 mol/mol and 2 mg/mL lipid concentration at 20°C or 4°C. Floatation assay was performed with polycarbonate centrifugation 11x34 mm tubes (Beckman Coulter, USA) and sucrose solutions prepared in HK buffer, i.e. 50 mM Hepes, pH 7.5, 150 mM NaCl. An aliquot of 150 µL of proteoliposomes was gently mixed with 100 µL of 60 % sucrose solution. Then, 200 µL of a second layer of 24% sucrose was added followed by 100 µL of HK buffer. Tubes were ultracentrifuged 90 minutes in a TLS-55 Swing bucket rotor (Beckman) at 55,000 rpm at 4°C with a slow acceleration and deceleration steps (5/5). Fractions were gently pipetted off with a syringe and analyzed by 4-12% NuPage gel after staining with Commassie Blue. Protein intensities and incorporation yield were measured with the Amersham Imager 680 and the analysis Software, version 2.0.0.

Protein orientation in the membrane of reconstituted proteoliposomes was determined from gel electrophoresis patterns before and after trypsin treatment of the reconstituted samples[63]. To this end proteoliposomes reconstituted with Alexa-488 labeled BmrA were reconstituted at 20°C or 4°C. Proteoliposomes were incubated at room temperature for 20 minutes in the presence of trypsin (trypsin/protein 1:1 w:w). The reaction was stopped by 2 µL of cOmplete™, EDTA-free Protease Inhibitor Cocktail. Since proteoliposomes were non permeable to trypsin, only proteins with NBDs pointing outward of vesicles were proteolyzed. Control experiments of proteolysis of all proteins was performed on Anapoe® X-100 solubilized proteoliposomes (Anapoe® X-100:lipid 2.5 w:w). Percent of protein orientation was determined from the ratio of the fluorescence intensities of the BmrA monomer band (M~ 65 000) before and after trypsin digestion (Amersham Imager 680 and analysis Software, version 2.0.0).

ATPase activity

ATP hydrolysis was carried out using a coupled enzyme assay of pyruvate kinase, and lactate dehydrogenase by absorbance changes of NADH/NAD+ ratio at 340 nm[37]. All measurements were made in triplicates. ATPase activity was measured in 50 mM MOPS pH 7.5, 150 mM NaCl, 10 mM of $MgCl_2$ with 1X enzyme cocktail and 0.5-1 µg of protein at 37°C in 150 µL total volume. Absorbance of NADH was measured by spectrometer (Cary Win 60 UV – Vis, Agilent Technologies) at 340 nm

every 15 s with quartz cuvette (N.105-254-15-40, Hellma Analytics, 3 x 3 mm). Proteoliposomes were incubated for 4 min at desired temperature. ATP was added at 1.5 or 5 mM final concentration and absorbance was recorded for 4 min but the first minute of reaction was ignored for ATPase activity calculation. Since the K_D of ATP for BmrA is 1 mM, this ensured that BmrA hydrolyzed ATP at maximum rate in all conditions[37]. Rate of inhibition was measured after addition of 2 mM of orthovanadate or 5 mM of AMP-PNP. ATPase activity was calculated by quantity of NADH oxidized equivalent to quantity of ATP hydrolyzed, per min and per mg of protein. ATP hydrolysis of BmrA in micelles of detergent was measured with Anapoe® X-100 0.05% in the cuvette. The amount of BmrA per assay was 1 µg for proteoliposomes and 2 µg for BrmA in detergent.

Cryo-electron microscopy and size measurement of proteoliposomes

Holey formvar lacey grids (Ted Pella, USA) were glow discharged for 30 s under vacuum. Then, 4 µL of 1 mg/mL of proteoliposomes were deposited during 30 s on the grid before flash frozen in liquid ethane with an EM-GP plunger (Leica Microsystems, Germany). Images were taken under low dose condition on a Glacios electron microscope (Thermofisher, USA) operating at 200 KV and recorded with a Falcon IVi camera. Diameter of proteoliposomes were measured manually from cryo-EM images from 594, 262 and 249 vesicles reconstituted at 20°C, 4°C with Apo BmrA and 4°C with ATP-Vi BmrA.

Proteoliposomes immobilization for smFRET experiments

A small channel of roughly 10 µL was custom-built between two coverslips (Menzel-Gläser, thickness #1): bottom coverslips is 25 mm diameter, and top squared-shaped coverslip is cut to 18×10 mm^2. The glass coverslips were placed on a Teflon carrier in a glass beaker. They were extensively washed under sonication with the following solutions: chloroform for 20 min (chloroform bath was then discarded and we allow slides to dry under the hood for 5 min), water for 5 min, KOH 1 M for 20 min, rinsed three times in water, and a final wash in water for 15 min. The coverslips were dried under a gentle stream of nitrogen and placed for 2 min in an air plasma cleaner. A double-sided tape mask was used to build the observation chamber. The channel was loaded by using a pipette tip on one side and aspirating at the other side with a clean paper towel Kimwipe. In order to specifically tether the proteoliposomes, the chamber was incubated with a solution of silane-PEG with 1% of silane-PEG-biotin at 5 mM for one hour. The chamber was rinsed by injecting 100 µL of buffer: 50 mM MOPS pH 7.5, 150 mM NaCl, 1 Mm $MgCl_2$. 40 µL of 20 µg/mL neutravidin was incubated for 5 to 10min. The surface was then rinsed with 100 µL of buffer. 40 µL of 1 mg/mL β-casein was incubated at least 10 min and then rinsed with 100 µL of buffer. Finally, 40 µL of proteoliposomes solution was injected at concentration 5.10^{-2} mg/mL and 5.10^{-3} mg/mL in lipids respectively for LV and SV. The solution was incubated for 5 to 10 min then rinsed with 100 µL of buffer before imaging.

Microscopy and smFRET assay

Observation was performed on a Nikon TI-Eclipse microscope equipped with a Nikon TIRF arm, a TIRF oil objective ×100 (NA 1.45, Nikon), a DualView system (Photometrics DV2) and an ORCA-Flash4.0 V3 Digital CMOS camera (Hamamatsu). The DualView system was equipped with a dichroic mirror 633 nm (ZT633rdc, Chroma) and the appropriate filters for the FRET couple sCy3/sCy5 (593/40 and 684/24 respectively, Chroma). We used alternating laser excitation (ALEX) at 532 nm (for sCy3 = donor) and 638 nm (for sCy5 = acceptor) (Lasers Oxxius). Acquisition rate was 1/200 ms^{-1}, with an exposure time of 50 ms in each channel with a 50 ms time-lag in between (necessary to overcome delay issues in our system).

All experiments were carried out utilizing an oxygen scavenging system supplemented with 1 mM Trolox as a photostabilization agent[43]. The oxygen scavenger system consists of 4 mg/mL D-glucose, 1 mg/mL glucose oxidase and 0.04 mg/mL catalase. A 10x D-glucose stock solution could be prepared and stored at -20°C for several months, and a 100x "gloxy" solution (mixture of catalase and glucose oxydase) was prepared and stored at 4°C for up to several months. The Trolox 2x stock solution is prepared at approximately 1-2 mM, with pH adjusted to 7.5, filtered at 0.2 µm and stored in the dark at 4°C up to two weeks. Solutions were mixed to a final 1x concentration at the last minute before observation (solution was filtered a last time at 0.2 µm before to load it in the observation chamber). It is worth noting that the oxygen scavenger system was more effective on the DNA sample, allowing us to observe minutes-long intensity traces, compared to the single-BmrA observation, for which the average fluorescence lifetime was 7 sec. Attempt to improve the photostability of the markers with another oxygen scavenger (PCD/PCA) was unsuccessful.

smFRET analysis

Data analysis was performed with the Matlab code iSMS[64,65], which allows to detect positions of Donor and Acceptor, to find matching pairs Donor/Acceptor by aligning the Donor and Acceptor channels and to output intensities I_D, I_F and I_A respectively in the Donor, FRET and Acceptor channels, of single molecules according to time (all intensities are corrected for background). The automatic bleach detection was used but could be manually adjusted if necessary and blinking intervals were set manually. In the software, the data evaluation process was then performed manually on Donor/Acceptor pairs. We discarded events with more than one bleaching step in either donor or acceptor channel, traces that showed very rapid photobleaching, or interference of strongly fluorescent neighbouring peaks (resulting in highly noisy intensity trace) were also excluded at this point. For each single molecule, the apparent FRET efficiency $E_{app} = (I_F) / (I_D + I_F)$ and the apparent stoichiometry $S_{app} = (I_D + I_F) / (I_D + I_F + I_A)$ were measured until either the donor or the acceptor bleaches, and were accumulated into a normalized histogram, without applying further corrections. Gaussian fits were performed in Matlab *Curve Fitter* tool. The following equation is used for the Gaussian fit on apparent FRET efficiency E_{app}: $a \times e^{-(E_{app} - <E_{app}>)^2/w^2}$ with a the amplitude, $<E_{app}>$ the mean position and w the parameter related to the Gaussian width. When double Gaussian fit was applied, the parameters of the fit were used to measure the probability to find the protein in low FRET state (= P_{op}) or in high FRET state (= P_{cl}). Errors were measured by applying bootstrapping on our data (10 times).

Theory

See theoretical section of the Supplementary Information.

References

1. Yang, X. *et al.* Structure deformation and curvature sensing of PIEZO1 in lipid membranes. *Nature* **604**, 377–383 (2022).

2. Haselwandter, C. A., Guo, Y. R., Fu, Z. & MacKinnon, R. Quantitative prediction and measurement of Piezo's membrane footprint. *Proc. Natl. Acad. Sci. U. S. A.* **119**, (2022).

3. Brohawn, S. G., Su, Z. & MacKinnon, R. Mechanosensitivity is mediated directly by the lipid membrane in TRAAK and TREK1 K+ channels. *Proc. Natl. Acad. Sci. U. S. A.* **111**, 3614–3619 (2014).

4. Cox, C. D., Bavi, N. & Martinac, B. Bacterial Mechanosensors. *Annu. Rev. Physiol.* **80**, 71–93 (2018).

5. Bavi, O. *et al.* Influence of Global and Local Membrane Curvature on Mechanosensitive Ion Channels: A Finite Element Approach. *Membranes (Basel).* **6**, 14 (2016).

6. Turner, M. S. & Sens, P. Gating-by-tilt of mechanically sensitive membrane channels. *Phys. Rev. Lett.* **93**, 118103 (2004).

7. Haselwandter, C. A., Guo, Y. R., Fu, Z. & MacKinnon, R. Elastic properties and shape of the Piezo dome underlying its mechanosensory function. *Proc. Natl. Acad. Sci. U. S. A.* **119**, (2022).

8. Markin, V. S. Lateral organization of membranes and cell shapes. *Biophys. J.* **36**, 1–19 (1981).

9. Corradi, V. *et al.* Lipid-Protein Interactions Are Unique Fingerprints for Membrane Proteins. *ACS Cent. Sci.* **4**, 709–717 (2018).

10. Schmidt, D. & MacKinnon, R. Voltage-dependent K+ channel gating and voltage sensor toxin sensitivity depend on the mechanical state of the lipid membrane. *Proc. Natl. Acad. Sci. U. S. A.* **105**, 19276–19281 (2008).

11. Aimon, S. *et al.* Membrane Shape Modulates Transmembrane Protein Distribution. *Dev. Cell* **28**, 212–218 (2014).

12. Quemeneur, F. *et al.* Shape matters in protein mobility within membranes. *Proc. Natl. Acad. Sci.* **111**, 5083–5087 (2014).

13. Kluge, C., Pöhnl, M. & Böckmann, R. A. Spontaneous local membrane curvature induced by transmembrane proteins. *Biophys. J.* **121**, 671–683 (2022).

14. Locher, K. P. Mechanistic diversity in ATP-binding cassette (ABC) transporters. *Nat. Struct. Mol. Biol.* **23**, 487–93 (2016).

15. Vasiliou, V., Vasiliou, K. & Nebert, D. W. Human ATP-binding cassette (ABC) transporter family. *Hum. Genomics* **3**, 281–290 (2009).

16. Januliene, D. & Moeller, A. Cryo-EM of ABC transporters: an ice-cold solution to everything? *FEBS Lett.* **594**, 3776–3789 (2020).

17. Thomas, C. *et al.* Structural and functional diversity calls for a new classification of ABC transporters. *FEBS Lett.* **594**, 3767–3775 (2020).

18. Orelle, C., Schmitt, L. & Jault, J. Waste or die : The price to pay to stay alive. *Trends Microbiol.* **31**, 233–241 (2022).

19. Zoghbi, M. E. & Altenberg, G. A. Luminescence resonance energy transfer spectroscopy of ATP-binding cassette proteins. *Biochim. Biophys. Acta - Biomembr.* **1860**, 854–867 (2018).

20. Galazzo, L. *et al.* The ABC transporter MsbA adopts the wide inward-open conformation in E.

coli cells. *Sci. Adv.* **8**, eabn6845 (2022).

21. Lacabanne, D. *et al.* Solid-State NMR Reveals Asymmetric ATP Hydrolysis in the Multidrug ABC Transporter BmrA. *J. Am. Chem. Soc.* **144**, 12431–12442 (2022).

22. Di Cesare, M. *et al.* The transport activity of the multidrug ABC transporter BmrA does not require a wide separation of the nucleotide-binding domains. *J. Biol. Chem.* **300**, 105546 (2024).

23. Fribourg, P. F. *et al.* 3D cryo-electron reconstruction of BmrA, a bacterial multidrug ABC transporter in an inward-facing conformation and in a lipidic environment. *J. Mol. Biol.* **426**, 2059–2069 (2014).

24. Dastvan, R., Mishra, S., Peskova, Y. B., Nakamoto, R. K. & Mchaourab, H. S. Mechanism of allosteric modulation of P-glycoprotein by transport substrates and inhibitors. *Science (80-.).* **364**, 689–692 (2019).

25. Chaptal, V. *et al.* Substrate-bound and substrate-free outward-facing structures of a multidrug ABC exporter. *Sci. Adv.* **8**, 1–11 (2022).

26. Orelle, C. *et al.* Conformational change induced by ATP binding in the multidrug ATP-binding cassette transporter BmrA. *Biochemistry* **47**, 2404–2412 (2008).

27. Lewinson, O., Orelle, C. & Seeger, M. A. Structures of ABC transporters: handle with care. *FEBS Lett.* **594**, 3799–3814 (2020).

28. Tang, Q. *et al.* Asymmetric conformations and lipid interactions shape the ATP-coupled cycle of a heterodimeric ABC transporter. *Nat. Commun.* **14**, (2023).

29. Liu, Y., Liu, Y., He, L., Zhao, Y. & Zhang, X. C. Single-molecule fluorescence studies on the conformational change of the ABC transporter MsbA. *Biophys. Reports* **4**, 153–165 (2018).

30. Husada, F. *et al.* Conformational dynamics of the ABC transporter McjD seen by single-molecule FRET. *EMBO J.* **37**, e100056 (2018).

31. Verhalen, B. *et al.* Energy transduction and alternating access of the mammalian ABC transporter P-glycoprotein. *Nature* **543**, 738–741 (2017).

32. Zoghbi, M. E. *et al.* Substrate-induced conformational changes in the nucleotide-binding domains of lipid bilayer-associated P-glycoprotein during ATP hydrolysis. *J. Biol. Chem.* **292**, 20412–20424 (2017).

33. Verhalen, B., Ernst, S., Börsch, M. & Wilkens, S. Dynamic ligand-induced conformational rearrangements in P-glycoprotein as probed by fluorescence resonance energy transfer spectroscopy. *J. Biol. Chem.* **287**, 1112–1127 (2012).

34. Levring, J. *et al.* CFTR function, pathology and pharmacology at single-molecule resolution. *Nature* **616**, 606–614 (2023).

35. Wang, L. *et al.* Characterization of the kinetic cycle of an ABC transporter by single-molecule and cryo-EM analyses. *Elife* **9**, 1–20 (2020).

36. Mehmood, S. *et al.* Structural and functional basis for lipid synergy on the activity of the antibacterial peptide ABC transporter McjD. *J. Biol. Chem.* **291**, 21656–21668 (2016).

37. Steinfels, E. *et al.* Characterization of YvcC (BmrA), a multidrug ABC transporter constitutively expressed in Bacillus subtilis. *Biochemistry* **43**, 7491–7502 (2004).

38. Mi, W. *et al.* Structural basis of MsbA-mediated lipopolysaccharide transport. *Nature* **549**, 233–237 (2017).

39. Pierman, B. *et al.* Activity of the purified plant ABC transporter NtPDR1 is stimulated by

diterpenes and sesquiterpenes involved in constitutive and induced defenses. *J. Biol. Chem.* **292**, 19491–19502 (2017).

40. Kapanidis, A. N. *et al.* Fluorescence-aided molecule sorting: analysis of structure and interactions by alternating-laser excitation of single molecules. *Proc. Natl. Acad. Sci. U. S. A.* **101**, 8936–41 (2004).

41. Deniz, A. A. *et al.* Single-pair fluorescence resonance energy transfer on freely diffusing molecules: observation of Förster distance dependence and subpopulations. *Proc. Natl. Acad. Sci. U. S. A.* **96**, 3670–5 (1999).

42. Hellenkamp, B. *et al.* Precision and accuracy of single-molecule FRET measurements—a multi-laboratory benchmark study. *Nat. Methods* **15**, 669–676 (2018).

43. Selvin, P. R. & Ha, T. *Single-molecule Techniques: A Laboratory Manual*. *CSHL Press* (2008).

44. Lee, W., Von Hippel, P. H. & Marcus, A. H. Internally labeled Cy3/Cy5 DNA constructs show greatly enhanced photo-stability in single-molecule FRET experiments. *Nucleic Acids Res.* **42**, 5967–5977 (2014).

45. Lacabanne, D. *et al.* ATP Analogues for Structural Investigations: Case Studies of a DnaB Helicase and an ABC Transporter. *Molecules* **25**, (2020).

46. Lacabanne, D. *et al.* Gradient reconstitution of membrane proteins for solid-state NMR studies. *J. Biomol. NMR* **69**, 81–91 (2017).

47. Javed, W. *et al.* Structural Insights into the Catalytic Cycle of a Bacterial Multidrug ABC Efflux Pump. *J. Mol. Biol.* **434**, (2022).

48. Li, M. J., Nath, A. & Atkins, W. M. Differential Coupling of Binding, ATP Hydrolysis, and Transport of Fluorescent Probes with P-Glycoprotein in Lipid Nanodiscs. *Biochemistry* **56**, 2506–2517 (2017).

49. Yan, Q., Shen, Y. & Yang, X. Cryo-EM structure of AMP-PNP-bound human mitochondrial ATP-binding cassette transporter ABCB7. *J. Struct. Biol.* **214**, (2022).

50. Marsh, D. Elastic curvature constants of lipid monolayers and bilayers. *Chem. Phys. Lipids* **144**, 146–159 (2006).

51. Tassis, K. *et al.* Single-molecule studies of conformational states and dynamics in the ABC importer OpuA. *FEBS Lett.* **595**, 717–734 (2021).

52. Yang, M. *et al.* Single-molecule probing of the conformational homogeneity of the ABC transporter BtuCD. *Nat. Chem. Biol.* **14**, 715–722 (2018).

53. Moeller, A. *et al.* Distinct Conformational Spectrum of Homologous Multidrug ABC Transporters. *Structure* **23**, 450–460 (2015).

54. Tonnesen, A., Christensen, S. M., Tkach, V. & Stamou, D. Geometrical membrane curvature as an allosteric regulator of membrane protein structure and function. *Biophys. J.* **106**, 201–209 (2014).

55. Ambudkar, S. V., Cardarelli, C. O., Pashinsky, I. & Stein, W. D. Relation between the turnover number for vinblastine transport and for vinblastine-stimulated ATP hydrolysis by human P-glycoprotein. *J. Biol. Chem.* **272**, 21160–21166 (1997).

56. Gustot, A., Smriti, Ruysschaert, J. M., Mchaourab, H. & Govaerts, C. Lipid composition regulates the orientation of transmembrane helices in HorA, an ABC multidrug transporter. *J. Biol. Chem.* **285**, 14144–14151 (2010).

57. Rigaud, J.-L. *et al.* Bio-Beads: an efficient strategy for two-dimensional crystallization of membrane proteins. *J. Struct. Biol.* **118**, 226–235 (1997).

58. Rigaud, J. L. & Lévy, D. Reconstitution of Membrane Proteins into Liposomes. *Methods Enzymol.* **372**, 65–86 (2003).

59. Rigaud, J. L., Pitard, B. & Levy, D. Reconstitution of membrane proteins into liposomes: application to energy-transducing membrane proteins. *BBA - Bioenerg.* **1231**, 223–246 (1995).

60. Lévy, D., Bluzat, A., Seigneuret, M. & Rigaud, J. L. A systematic study of liposome and proteoliposome reconstitution involving Bio-Bead-mediated Triton X-100 removal. *BBA - Biomembr.* **105**, 179–190 (1990).

61. Rigaud, J.-L., Lévy, D., G, M. & Lambert, O. Detergent removal by Bio-Beads. Application to membrane protein reconstitution and two-dimensional crystallisation. *Eur J. Biophys.* **27**, 305–319 (1998).

62. Mesmin, B. *et al.* XA four-step cycle driven by PI(4)P hydrolysis directs sterol/PI(4)P exchange by the ER-Golgi Tether OSBP. *Cell* **155**, 830 (2013).

63. Lévy, D., Guiik, A., Bluzat, A. & Rigaud, J.-L. Reconstitution of the sarcoplasmic reticulum Ca2+-ATPase: mechanisms of membrane protein insertion into liposomes during reconstitution procedures involving the use of detergents. *Biochim. Biophys. Acre* **1107**, 283–298 (1992).

64. Preus, S., Noer, S. L., Hildebrandt, L. L., Gudnason, D. & Birkedal, V. iSMS: single-molecule FRET microscopy software. *Nat. Methods* **12**, 593–594 (2015).

65. Hildebrandt, L. L., Preus, S. & Birkedal, V. Quantitative single molecule FRET efficiencies using TIRF microscopy. *Faraday Discuss.* **184**, (2015).

Acknowledgements
We thank Raju Regmi, Elie Balloul and Nikos Hatzakis (University of Copenhagen) for support for the data analysis and insightful discussions. We thank Julien Maufront for analysis of the cryo-images of proteoliposomes. We thank Bassam Hajj, Julien Pernier and Xavier Solinas (Ecole Polytechnique) for technical support and David Lacoste (ESPCI), Peter Tieleman, Estefania Barreta Ojeda (University of Calgary) for providing conceptual ideas.
PB is member of the CNRS consortium AQV. AD, SJP, MD, PS, DL and PB are members of the Labex Cell(n)Scale (ANR-11-LABX0038) and Paris Sciences et Lettres (ANR-10-IDEX-0001-02). We acknowledge the Cell and Tissue Imaging Core facility (PICT IBiSA), Institut Curie, member of the French National Research Infrastructure France-BioImaging (ANR10-INBS-04).

Funding: This work was supported by:
Agence Nationale pour la Recherche : ANR-16-CE11-0026-01
Doctoral school EDPIF (ED564, Paris) for AD
Doctoral school ED CDV (ED 515, Paris) and PSL for SJP
Agence Nationale pour la Recherche : ANR-19-CE11-0002-01 for RKS and PS

Author contributions: MD, PB, DL and AD planned and designed the research. SJP, JM and DL purified the protein, optimized the liposome reconstitution. SJP, ADC and DL performed the cryo-EM images and ATPase activity measurements. AD and MD set up and optimized the single molecule FRET assay and sample preparation. AD performed the smFRET experiments and analysis. RKS and PS developed the theoretical model and performed the fit to the experimental data. AD, PB, DL and PS wrote the manuscript. EM and MC reviewed and commented on the manuscript.

Competing interests: Authors declare that they have no competing interests.

Data and materials availability: All data needed to evaluate the conclusions in the paper are present in the paper and/or the Supplementary Materials.

Figures and Tables

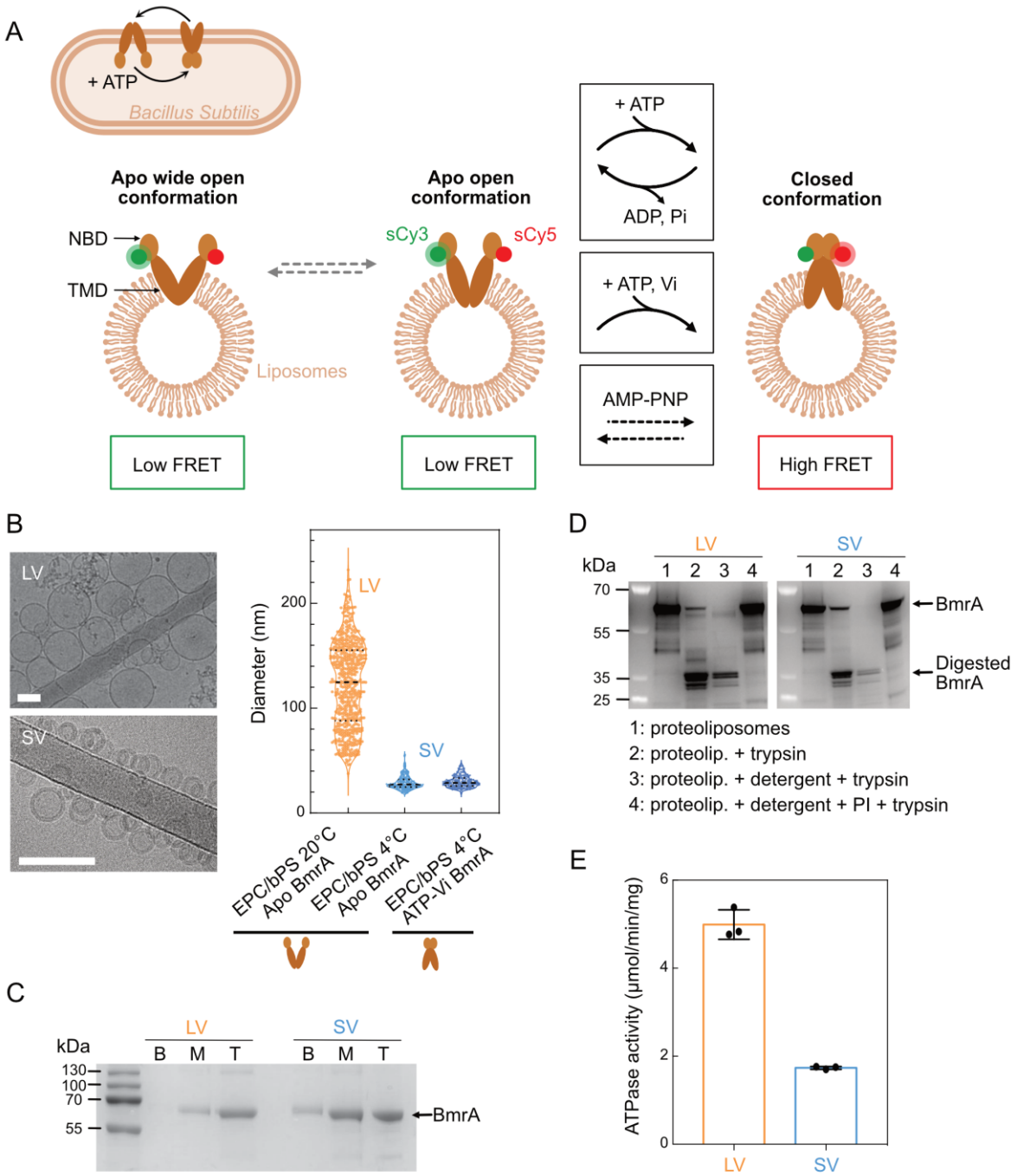

Figure 1. Increasing membrane curvature reduces BmrA ATPase activity. (A) Schematic representation of the two conformations of BmrA in *Bacillus Subtilis* (top left) and reconstituted in opposite orientation in liposomes (bottom): the open and wide-open, or apo, conformations, (inward-facing in bacteria) and the closed conformation (outward-facing). The green and red disks indicate the labelling position of sCy3 (donor) and sCy5 (acceptor) for smFRET experiments. The conformational change between apo and closed states occurs actively upon hydrolysis of ATP (top box); it is also possible to covalently trap BmrA in the closed conformation by adding ATP and Vanadate (Vi) (middle box); finally, a non-hydrolyzable form of ATP, AMP-PNP, binds to NBDs and leads to a passively reversible protein closing (bottom box). **(B)** Left: Cryo-EM images of EPC:bPS (90:10 w/w) proteoliposomes (apo BmrA) obtained at two different reconstitution temperatures, T=20°C for the LV

and T=4°C for the SV. Cryo-EM was used to characterize both the unilamellarity of the vesicles and their size distribution (scale bar: 50 nm). Right: Distribution of liposome sizes deduced from cryo-EM. Two different populations are obtained: average diameter ø=123 ± 41 nm (n = 594) for LV (Orange) and ø=29 ± 6 nm for SV, independently of the conformation of the protein incorporated, either open (apo, light blue, n=262) or closed (ATP-Vi, dark blue, n=249). **(C)** Characterization of protein incorporation in vesicles LV (left) and SV (right) using a floatation assay in a sucrose gradient. Bottom (B), middle (M) and top (T) fractions are run on a NuPage gel. Intensity in the bottom fraction reveals very little protein aggregation, indicating that BmrA is properly incorporated in liposomes. **(D)** Characterization of protein orientation in vesicles LV (left) and SV (right), by cleaving the NBDs with trypsin. Alexa 488-labelled BmrA is reconstituted in LV or in SV, and the proteoliposome sample is run on the gel intact (1) and after 20 min incubation with 0.6 µg trypsin (2). Addition of detergent (det.) allows to resolubilize the proteoliposomes. This sample is run on the gel after 20 min incubation with 0.6 µg trypsin (3) and in presence of protease inhibitor (PI, used to stop the action of trypsin after 20min) and with 0.6 µg trypsin (4). Column 3 shows that solubilized BmrA is digested by trypsin. Column 4 reveals the efficiency of the protease inhibitor on trypsin. Column 2 shows that, both in LV and SV, BmrA is 85% and 75%, respectively, oriented with NBD pointing outside. This characterization shows that the protein has an orientation in liposomes opposite to bacteria (as represented in panel A). **(E)** Effect of the liposome size on the protein ATPase activity (in µmol of ATP consumed per min per mg of protein), in the presence of 5 mM of ATP at 37°C (3 measurements).

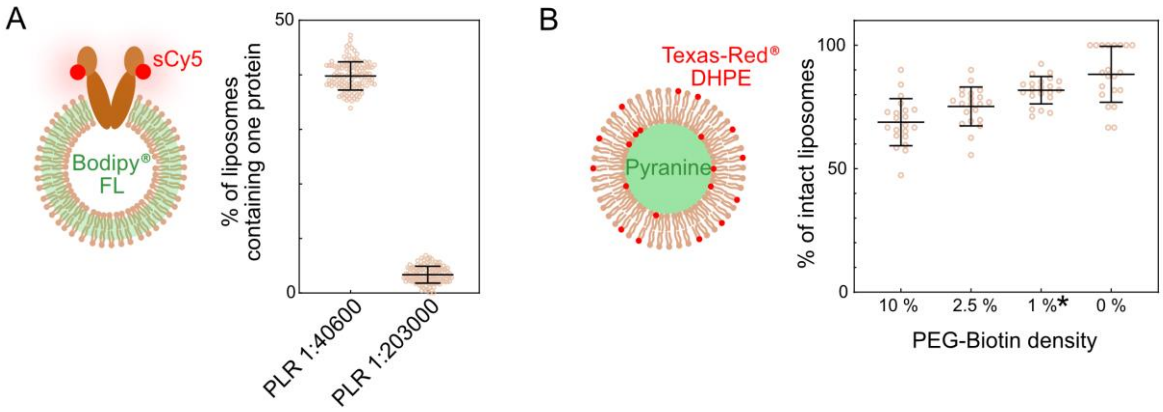

Figure 2. Liposomes contain at most one protein copy and remain impermeable upon surface tethering. (A) Control of the single molecule regime in SV, using a double labeling of the protein and of the liposome membrane. Left: Scheme of the experiment. sCy5-labelled BmrA is reconstituted in SV that contain 0.01% fluorescent lipids (Bodipy®-FL). Colocalization of sCy5 and Bodipy®-FL signals indicates a liposome containing at least one protein. Right: Percentage of liposomes (per image) containing at least one BmrA, for two different PLR, 1:203000 and 1:40600. In both cases, most liposomes are empty. 120 images were analyzed. **(B)** Control of the integrity of the liposomes after immobilization on the coverslip. Left: Liposomes containing 0.5% DHPE-Texas Red® lipids and the soluble dye pyranine in their lumen are incubated for 5min in the chamber. Potential rupture of the liposomes due to the adhesion via the PEG-biotin neutravidin interaction is detected via the fluorescence signal: intact liposomes correspond to colocalization of the green and red signals. Right: fraction of intact liposomes (per image) as a function of the PEG-biotin density on the surface, 10, 2.5, 1 and 0%. The optimal condition is obtained at 1% (*), which has been used in the whole study. 21 images were analyzed.

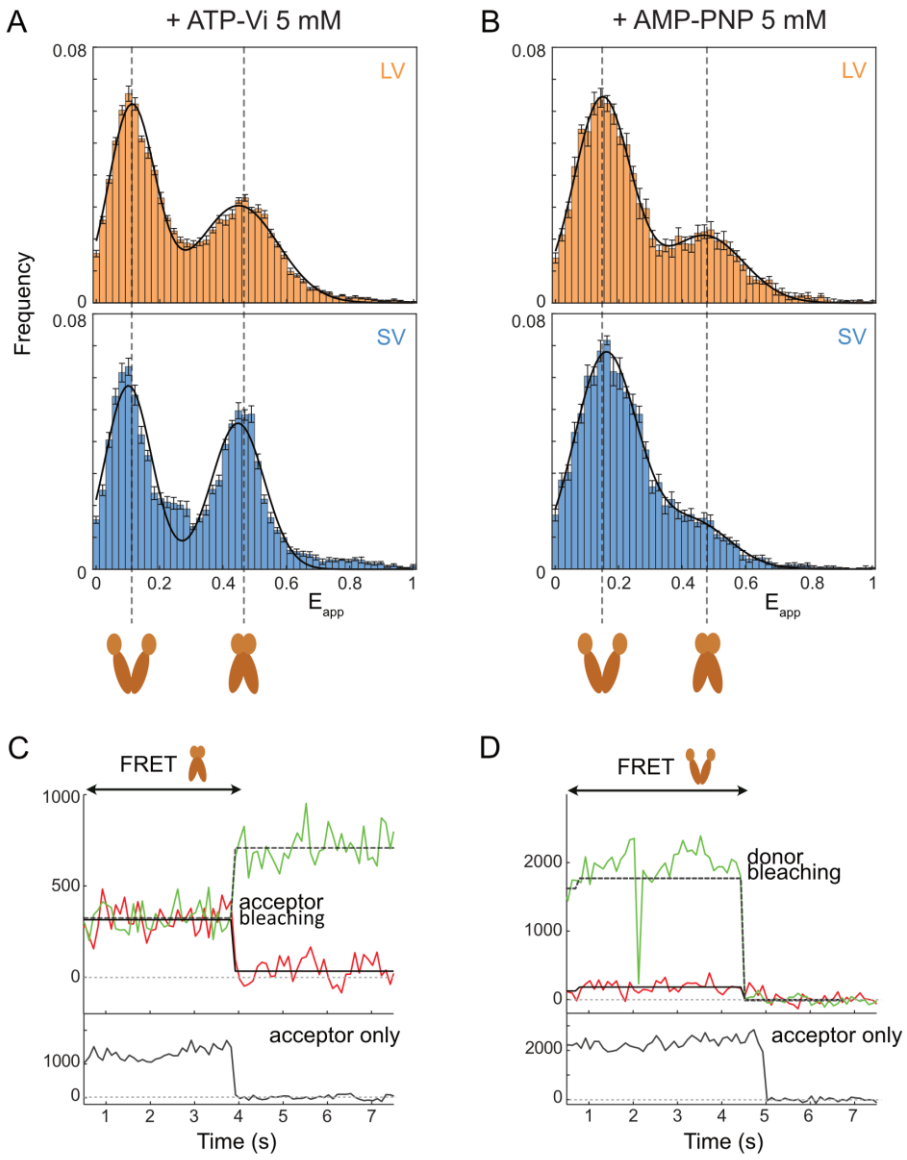

Figure 3. smFRET shows that BmrA closed conformation depends on membrane curvature in the presence of non-hydrolysable ATP. (A,B) Cumulated histograms of apparent FRET efficiency E_{app} upon addition of (A) ATP-Vi 5 mM in LV (top) and SV (bottom) (B) 5 mM AMP-PNP in LV (top) and SV (bottom). The thick line corresponds to the two-gaussian fit. N_{all}: number of time points in histograms, N_{prot}: corresponding number of proteins. (A top) N_{all} = 18559 and N_{prot} = 525. (A bottom) N_{all} = 7552 and N_{prot} = 325. (B top) N_{all} = 5109 and N_{prot} = 157. (B bottom) N_{all} = 5094 and N_{prot} = 141. For each condition, data come from two independent experiments. Error bars are calculated using bootstrapping. **(C,D)** Typical time traces of proteins in LV with ATP-Vi 5mM (C) in closed state and (D) in open state. Top panel shows donor (green) and FRET (red) intensities over time. Plain and dashed line represent a fit of the FRET switches. Bottom panel shows the intensity of acceptor only (black).

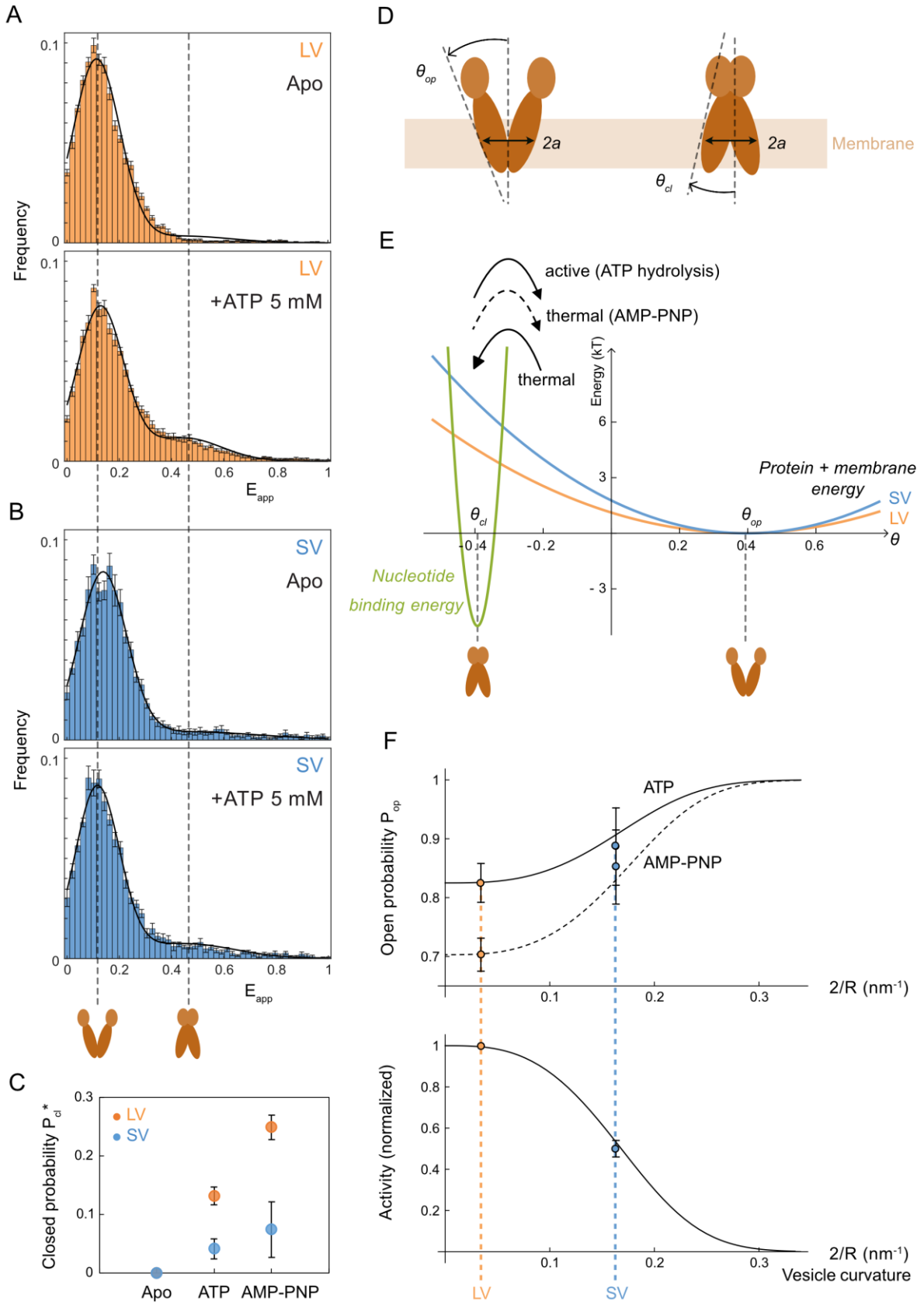

Figure 4. Effect of curvature on conformation and function of BmrA. (A,B) Cumulated histogram of apparent FRET efficiency E_{app} for BmrA in apo conformation in LV (top A) and SV (top B), and in

the presence of 5 mM Mg-ATP in LV (bottom A) and SV (bottom B). The thick line corresponds to a two-gaussian fit where the position of the high-FRET peak is set to $<E_{app}>_{HF}$ in ATP-Vi. (top A) N_{all} = 10451 and N_{prot} = 310. (bottom A) N_{all} = 7743 and N_{prot} = 226. (top B) N_{all} = 2797 and N_{prot} = 115. (bottom B) N_{all} = 3959 and N_{prot} = 130. For each condition, data come from two independent experiments, except SV Apo (top B) from three. Error bars are calculated using bootstrapping. **(C)** Probability for the protein to be in closed state P_{cl}* (P_{cl}* = P_{cl} – P_{cl}(apo) where P_{cl}(apo) corresponds to the high FRET fraction detected in apo state) as a function of nucleotide and liposome size. Error bars are calculated from the errors on P_{cl} obtained with bootstrapping (Table 2). **(D)** Definition of the geometrical parameters 2a, θ_{op} and θ_{cl} used in the theoretical model. **(E)** Scheme of the two-state model. The energy landscape for the protein alone favors the open state. In the presence of nucleotides, NBDs dimerize, and an additional energy contribution (green) favors the closed state. The membrane energy adds a contribution that further disfavors the closed state, all the more as for the SV (blue) than for the LV (orange). The open-to-closed transition is thermal, while the closed-to-open is either thermal (non-hydrolysable AMP-PNP)) or triggered by ATP hydrolysis. **(F)** Results of the model for the probability of being in the open conformation (top, with ATP or AMP-PNP) and the activity (bottom, ATP turnover rate), as a function of the curvature of the SUVs. Dots corresponds to experimental data P_{op} from smFRET (top) and from ATPase assay (bottom). Both the opening probability and the activity curves were fitted with a single parameter κ=21 kT. For the probability data (top), the error bar corresponds to the noise measured at high FRET value in Apo conformation (see Table 2). For the activity data (bottom), the error bar corresponds to the standard deviation calculated from various measurements.

		a_{LF}	$<E_{app}>_{LF}$	w_{LF}	a_{HF}	$<E_{app}>_{HF}$	w_{HF}
LV	ATP-Vi	0.062	0.11	0.10	0.030	0.45	0.18
	AMP-PNP	0.064	0.15	0.13	0.021	0.47	0.17
	Apo	0.091	0.11	0.13	0.0034	0.45 (fix)	0.26
	ATP	0.077	0.13	0.13	0.012	0.45 (fix)	0.20
SV	ATP-Vi	0.058	0.10	0.10	0.046	0.45	0.12
	AMP-PNP	0.067	0.16	0.14	0.015	0.43	0.16
	Apo	0.082	0.14	0.13	0.0042	0.45 (fix)	0.41
	ATP	0.085	0.12	0.12	0.0075	0.45 (fix)	0.27

Table 1. Two-gaussian fit parameters of BmrA smFRET histograms. Amplitude *a*, mean $<E_{app}>$, and width parameter *w* for the Low-FRET (LF) and High-FRET (HF) peaks.

		P_{op} (%)	P_{cl} (%)
LV	ATP-Vi	52.7 ± 0.3	47.3 ± 0.3
	AMP-PNP	67.5 ± 1.5	32.5 ± 1.5
	Apo	92.3 ± 0.6	7.7 ± 0.6
	ATP	79.2 ± 0.9	20.8 ± 0.9
SV	ATP-Vi	50.3 ± 1.2	49.7 ± 1.2
	AMP-PNP	78.9 ± 3.8	21.1 ± 3.8
	Apo	86.2 ± 0.7	13.8 ± 0.7
	ATP	82.1 ± 1.0	17.9 ± 1.0

Table 2. Fractions of proteins in open (*op*) and closed (*cl*) states for the two vesicle populations LV and SV. Calculated from the parameters of Table 1, the Low-FRET parameters correspond to the open conformation, and High-FRET to the closed state.